



**Magnon hybridization of vortices with opposite chirality in magnetic thin films**Chaozhong Li,<sup>1,\*</sup> Zhengyi Li,<sup>2,\*</sup> Mangyuan Ma,<sup>2</sup> Yuping Yao,<sup>1</sup> Huige Ma,<sup>4</sup> Changjun Jiang <sup>1</sup>, C. K. Ong,<sup>1,3</sup>  
Fusheng Ma,<sup>2,†</sup> and Guozhi Chai <sup>1,‡</sup><sup>1</sup>Key Laboratory for Magnetism and Magnetic Materials of Ministry of Education, School of Physical Science and Technology, Lanzhou University, Lanzhou 730000, China<sup>2</sup>Jiangsu Key Laboratory of Opto-Electronic Technology, School of Physics and Technology, Nanjing Normal University, Nanjing 210046, China<sup>3</sup>Department of Physics, Xiamen University Malaysia, Jalan Sunsuria, Bandar Sunsuria, 43900 Sepang, Selangor, Malaysia<sup>4</sup>Beijing Institute of Nanoenergy & Nanosystems, Chinese Academy of Sciences, Beijing 101400, China

(Received 7 February 2024; revised 12 May 2024; accepted 9 June 2024; published 25 June 2024)

We have proposed and demonstrated the hybridization between magnon modes of a magnetic vortex pair (MVP) of opposite chirality. The proposed magnon hybridization in MVP configurations of opposite chirality is realized by micromagnetic simulations. It is found that the hybridization results from the coupling between the breathing mode originating from the individual motion of a single magnetic vortex and the collective mode arising from the overall behavior of the MVP. Then the hybridization of different magnon modes is experimentally observed in the CoZr striped domain thin film systems, in which the MVP configuration exists. Moreover, the hybridization, coupling field, and strength can be modulated by the thickness of the CoZr films, i.e., the dimension of the magnetic vortex. Finally, we investigate the effect of different magnetic parameters on the magnon hybridization, i.e., the exchange constant, perpendicular magnetic anisotropy constant, and saturation magnetization. Our results may deepen the understanding of the hybridization phenomenon of magnons for complex magnetic textures.

DOI: [10.1103/PhysRevB.109.214437](https://doi.org/10.1103/PhysRevB.109.214437)**I. INTRODUCTION**

Hybridization in magnonic systems combines the advantages of magnons of different modes (low energy consumption, high coherence, the ability to carry different angular momentum, etc.) to provide a promising solution for coherent information storage [1–5]. Hybridization between magnons facilitates the magnonic application of coherence for information transfer and processing in quantum information and quantum computing [6–10]. Magnon hybridization has been extensively investigated in many magnetic systems, such as in ferromagnetically coupled multilayer systems [11–14], synthetic ferrimagnetic/antiferromagnetic systems [15–17], and single-crystal magnetic thin film systems [18,19]. In recent years, magnetic textures have attracted special attention due to their potential applications in high-density magnetic data storage [20], magnetic field sensors [21], and logic computing devices [22,23]. Nowadays, vortices are seen at all scales, not only in superconductors and quantum fluids but also in a typical magnetic texture [24–28]. Furthermore, vortices have been found to have a strong influence on the properties of many materials, including superconductors and ferromagnets [29–34]. Li *et al.* [27] and Luk'yanchuk *et al.* [28] discovered polar vortices in electrically polarized materials, i.e., a

ferroelectric superlattice, and investigated the dynamics of these polarization patterns. However, the hybridization phenomenon of magnon of vortices in magnetic materials has not been fully investigated.

Different from the single-domain state, the complex magnetic structure (e.g., magnetic vortex and skyrmion) has a special magnetic moment distribution and an intrinsic excitation spectrum, so the dynamics under the applied magnetic field are more complex. Due to the different dispersion relationships of different spin-wave modes in magnetic vortices [35] or breathing and rotation modes in skyrmion lattices [36–38], there should also exist regions of dispersion crossover, which could result in mode hybridization. Consequently, here, we consider a magnetic vortex pair (MVP) comprising two magnetic vortices with either the same or opposite chirality, left- and right-handed magnetic vortices [39,40], as schematically shown in Figs. 1(a) and 1(b). There are two types of magnon modes with different dispersions for the MVP. For an individual vortex, the breathing mode [36,41], as shown in (i) of Fig. 1(c), each magnetic vortex nucleus expands and shrinks temporally. For the MVP, on the other hand, a collective behavior will present, where all the magnetic vortices swing out-of-phase or in-phase from side to side regularly for MVPs with the same or opposite chirality, as shown in (ii) and (iii) of Fig. 1(c), respectively. In other words, MVPs have different magnon modes depending on the comprising vortex with the same or opposite chirality. The frequency of the breathing (collective) mode is inversely (positively) dependent on the external magnetic field. Therefore, a

\*These authors contributed equally to this paper.

†Contact author: phymafs@njnu.edu.cn

‡Contact author: chaigzh@lzu.edu.cn

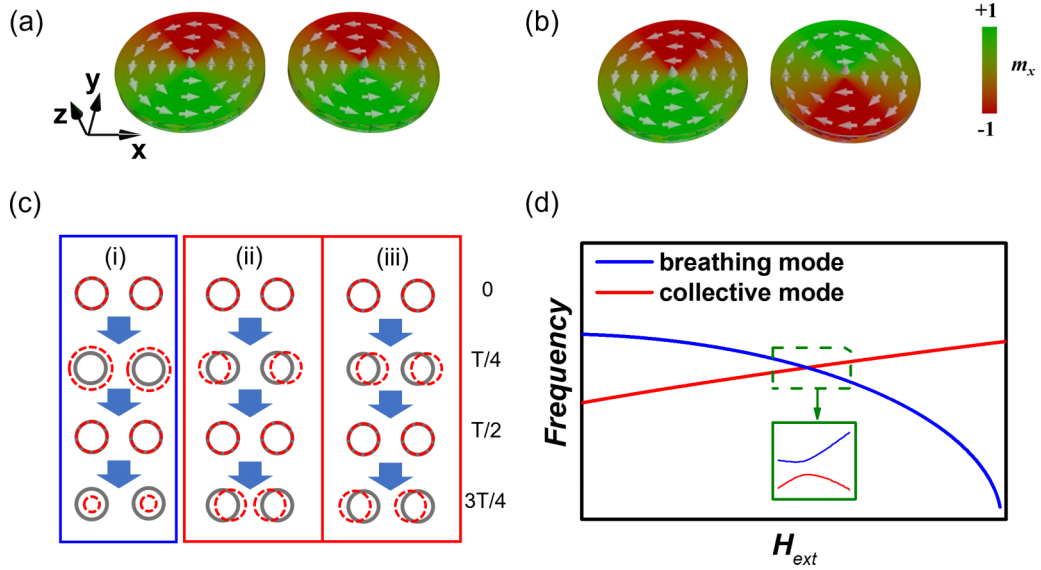


FIG. 1. Schematic diagram of the magnetic vortex pair (MVP): (a) the same chirality and (b) the opposite chirality. The external and excitation fields are along the  $z$  direction. (c) Schematic diagram of magnon modes: (i) the breathing mode of individual vortex; the collective mode of the MVP with (ii) the same and (iii) opposite chirality. (d) Frequency-field dispersion relation for bare magnon modes. Inset presents the anticrossing resulting from the hybridization.

hybridization between these two magnon modes is expected, as schematically shown in Fig. 1(d). Therewith, we realized magnon hybridization for MVPs with opposite chirality by micromagnetic simulations. From the experimental point of view, arrays of chiral opposite MVPs exist, while arrays of the same chiral MVPs cannot stably exist due to the strong exchange interaction of the spins between the MVPs (for more details, see Fig. S2 in the Supplemental Material (SM) [42]; Fig. S1 in the SM [42] shows the simulation results of the single magnetic vortex).

Subsequently, the numerically observed phenomenon of magnon hybridization is experimentally demonstrated in magnetic thin films with MVP configuration. In striped domains, the arrangement of the magnetic moments is vortexlike since the stripes in striped domain films are separated by a Bloch wall in the center and a Néel wall on the film surfaces. Consequently, analogizing to polar vortices [27,28], we would use a magnetic vortex to describe the magnetization distribution at the cross-section of striped domain structures. Previously, it was found that different dynamic resonance modes existed in magnetic thin film systems with striped domains [43–49]. For example, Camara *et al.* [49] investigated multiple eigenmodes in the evolution of striped domains in an  $\alpha'$ -FeN thin film by using different techniques and experimental configurations. The evolution of these modes is accompanied by different spatial localizations in specific regions, such as closure domains at the surface of the stripes and bulk domains inside the stripe. Here, from the view of different modes of the overall precession of the magnetic moment, we investigate the hybridization of different magnon modes by employing CoZr striped domain thin film systems with MVP structure.

## II. MICROMAGNETIC SIMULATION

Micromagnetic simulations are performed by using MUMAX3 [50]. The simulated structure has dimensions of  $200 \times$

$200 \times 10 \text{ nm}^3$  along the  $x$ ,  $y$ , and  $z$  axes, as shown in Fig. 2(a), respectively, and is divided into  $80 \times 80 \times 1$  cells. Periodic boundary conditions are applied along the  $x$  and  $z$  axes. The magnetic parameters used are as follows:  $M_s = 8 \times 10^5 \text{ A/m}$ , exchange constant  $A = 1.0 \times 10^{-11} \text{ J/m}$ , and damping constant  $\alpha = 0.01$ . The perpendicular magnetic anisotropy constant  $K_u$  is set to  $2.8 \times 10^4 \text{ J/m}^3$  along the  $y$  axis. The static magnetization is relaxed from a pair of magnetic vortices with opposite chirality. To excite the magnon modes of vortices, a driving field  $h(t) = h_0 \sin[2\pi f_c(t - t_0)]/[2\pi f_c(t - t_0)]$  is applied along the  $z$  axis, where the cutoff frequency  $f_c = 100 \text{ GHz}$ , the offset time  $t_0 = 0.05 \text{ ns}$ , and the amplitude  $h_0 = 5 \text{ mT}$ . The magnonic spectra can be obtained by performing the Fourier transform of the  $x$  component of the spatially averaged magnetization  $m_x(t)$ .

Figure 2(a) shows the static magnetization distribution of MVPs with opposite chirality in our simulation, and the distance between adjacent magnetic vortices is  $d$ . To simulate the actual situation,  $d = 0$  here, and the simulation results of other  $d$  are shown in Figs. S2(f)–S2(j) in the SM [42]. The simulated  $f$ - $H$  dispersions under the longitudinal excitation, i.e., the applied magnetic field is parallel to the microwave magnetic field, are presented in Fig. 2(b). An anticrossing character is observed at  $\mu_0 H = 12.8 \text{ mT}$ . Since coupling appears at the cross point of the breathing mode (blue dashed line) and collective mode (orange dashed line) of vortices, we speculated that the coupling is attributed to the hybridization of the above two magnon modes. The strength of the hybridization between the two resonances is defined as the coupling strength  $g/2\pi$ . By Lorentzian fitting of the simulated original spectral (see Fig. S3 in the SM [42]), we can obtain  $g/2\pi = (\Delta f/2)_{\min} = 0.48 \text{ GHz}$ , where  $\Delta f$  is the difference between the frequencies of the two magnon modes. To clarify the formation of coupling, we calculate four profiles of the vortex mode at selected fields and frequencies marked as I–IV

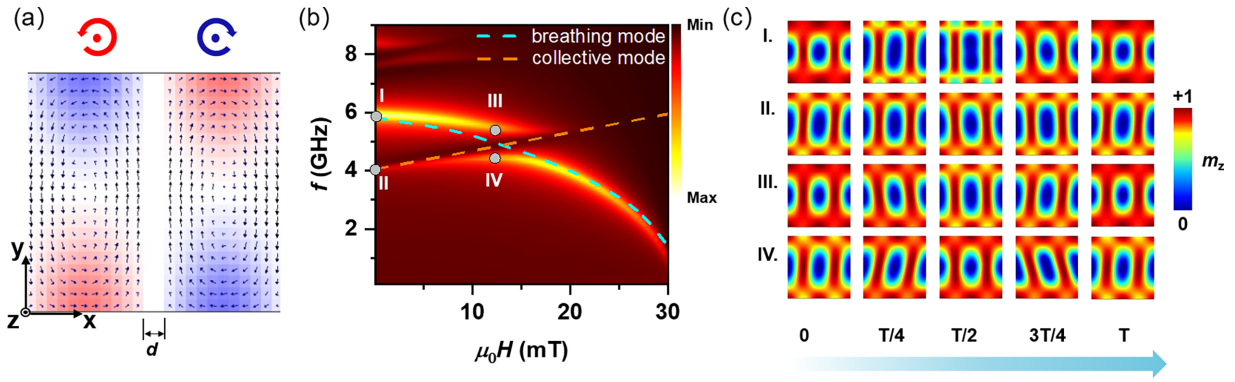


FIG. 2. (a) Static magnetization distribution of magnetic vortex pair (MVP) with opposite chirality. The external field is along the  $z$  direction. (b) Contour plots of simulated  $f$ - $H$  dispersion under the longitudinal excitation. The level repulsion with splitting  $g/2\pi = 0.48$  GHz is observed at  $\mu_0 H = 12.8$  mT. The blue and orange dashed lines indicate bare breathing and collective modes, respectively. (c) Temporal snapshots of magnon mode of MVP of opposite chirality at various  $H$  and  $f$  as marked in (b) by I–IV.

in Fig. 2(b). For mode I, as shown in the first row of Fig. 2(c), the breathing mode is observed where the area of each vortex expands and shrinks dynamically. For mode II, as shown in the second row of Fig. 2(c), the collective mode is observed where each vortex swings in-phase. As shown in the last two rows of Fig. 2(c), mode III/IV exhibits a superimposed pattern of the breathing and collective modes in one period. Modes III and IV are hybridized between I and II. From simulated results, for the magnetic film with magnetic vortex structures having two magnon modes at zero field, the high-frequency branch originates from the breathing mode generated by the motion of a single magnetic vortex, and the low-frequency branch derives from the collective mode induced by the whole motion of all the magnetic vortices, and both modes are present in the hybridized region.

### III. EXPERIMENTAL RESULTS

Next, we experimentally studied the magnon hybridization of the MVP configuration in CoZr thin film with striped domains by using ferromagnetic resonance (FMR) measurement. A series of CoZr thin films was prepared with various thicknesses of 180, 210, 240, 270, and 300 nm, which were magnetron sputtered on single-crystal Si (100) substrates. The magnetization hysteresis loops and magnetic domain images for the samples of different thicknesses are shown in Fig. S5 in the SM [42]. (The basic magnetic parameters for all the samples are gathered in Table S1 in Sec. S6 in the SM [42].) The dynamic magnetic characterization of the samples, i.e., frequency-dependent permeability spectra, was measured by using a vector network analyzer (Agilent PNA E8363B, USA) equipped with a short-circuited microstrip line at room temperature [51,52], which covers the frequency range of 0.1–9 GHz. The setup of FMR measurement is schematically shown in Fig. 3(a), with the long brown bar as the microstrip line. We saturated the sample beforehand and then placed it on the microstrip line under the state of remanent magnetization to ensure that the applied magnetic field was parallel to the direction of the MVPs. By varying the angle  $\theta$  between the microwave and the applied magnetic field in Fig. 3(a), we performed measurements with longitudinal,  $45^\circ$ , and transverse excitations, i.e.,  $\theta$  was  $0^\circ$ ,  $45^\circ$ , and  $90^\circ$ , respectively,

where the longitudinal excitation allows modes in which the amplitude of the magnetic moments cancel each other and still couple with the microwave field and resonate with significant absorption peaks [53].

To measure the magnon hybridization phenomena, we have conducted a systematic study of CoZr thin film with thickness of 240 nm. The magnetic force microscope (MFM) measured magnetic domain image of CoZr thin films in the remanent magnetization state is shown in Fig. 3(b); this is consistent with our previous result [54]. The color code represents the value of the resonant frequency  $\Delta f$  of the scanning probe in the MFM, reflecting the magnitude of the out-of-plane component. Then we measured the permeability spectra under different experimental configurations (different  $\theta$ ) and magnetic fields using the setup as shown in Fig. 3(a). The imaginary parts of the permeability spectra for several representative magnetic fields under the longitudinal excitation are shown in Fig. 3(c); all the spectra under different magnetic fields have two resonance peaks. With the magnetic field increasing, the two modes move gradually close to each other and reach the minimum at 17.95 mT, and then the two modes gradually separate again. The amplitudes of the two resonance peaks are exchanged along with the magnetic field. To present the hybridization phenomenon of the two modes in the MVP array more intuitively, we carried out measurements of the permeability spectra under the denser swept magnetic field of the 240 nm CoZr thin film, as shown in Figs. 3(d)–3(f). From Fig. 3(d), an obvious anticrossing of the two modes is observed at 17.95 mT, and  $g/2\pi = 0.70$  GHz, i.e., the two modes undergo hybridization under a certain magnetic field. The  $g/2\pi$  is greater than the relaxation rate (frequency linewidth) of the two magnon modes far away from the avoided crossing. Therefore, the coupling is recognized as strong coupling in this paper. (More details can be found in Fig. S4 in the SM [42].) These results are qualitatively consistent with the observations of simulation shown in Fig. 2. In addition, we changed the relative orientations of the microwave magnetic field and the magnetic domains (i.e., the external magnetic field). Under transverse excitation [Fig. 3(f)] at zero field, both modes increase with

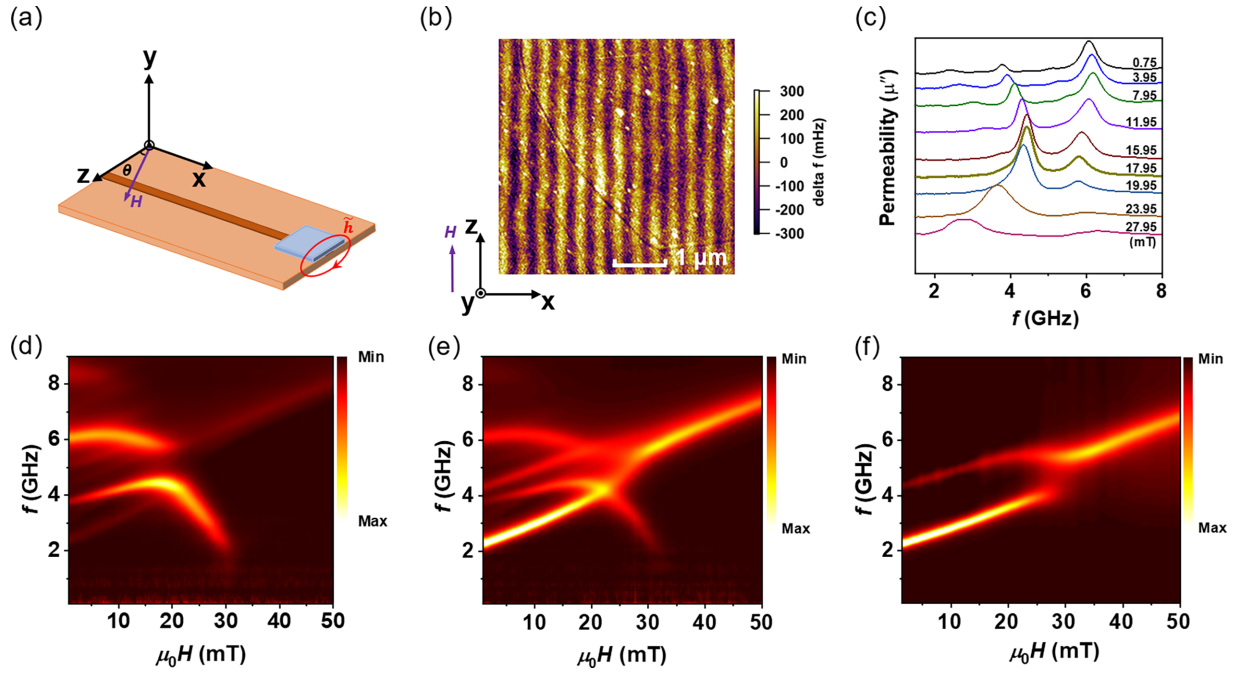


FIG. 3. (a) Schematic diagram of the ferromagnetic resonance (FMR) measurement, where  $\theta$  is the angle between the applied magnetic field and the microwave magnetic field. (b) The measured magnetic force microscope (MFM) image of the CoZr thin film with thickness of 240 nm at zero field. The colors represent the values of  $\Delta f$  obtained from MFM measurements and indicate the magnitude of the out-of-plane component of the film magnetization. (c) Representative spectra measured at different magnetic fields under the longitudinal excitation. Contour plots of permeability spectra of the CoZr thin film with thickness of 240 nm under different  $\theta$ : (d)  $0^\circ$ , (e)  $45^\circ$ , and (f)  $90^\circ$ .

the magnetic field and eventually merge into one mode. Micromagnetic simulation results indicate that the hybridization under transverse excitation may come from the hybridization of the breathing accompanying the relative motion in the  $y$  direction and collective mode (details are given in Sec. S5 in the SM [42]). When  $\theta$  is  $45^\circ$ , as shown in Fig. 3(e), the pure superposition of the mode hybridization phenomenon under longitudinal and transverse excitation, i.e., the hybridization, does not occur between the longitudinal and transverse excitation configurations.

#### IV. DISCUSSION

Comparing Figs. 3(d)–3(f), we can see that, under longitudinal excitation [Fig. 3(d)], there are some weaker modes such as 2.4 and 5 GHz and a higher-frequency mode for larger magnetic fields, which mainly originate from the projection of the low-frequency branch and are identical to the corresponding modes under transverse excitation. The reason is that it is difficult in nature to ensure the microwave and the applied magnetic field are completely parallel and the orientation of the magnetic domains is completely consistent during the experiments. This can be confirmed by both the absence of these weaker peak in the results of simulations [Fig. 2(b)] and the other thickness samples in Fig. 4 under longitudinal excitation.

For CoZr thin films, different thicknesses correspond to different sizes of magnetic vortices. Therefore, we have also performed measurements on CoZr thin films with different thicknesses, as shown in Figs. 4(a)–4(e). For all five samples,

two resonance modes are observed at zero magnetic field with the presence of anticrossing in the  $f$ - $H$  dispersion. Hence, the robustness of the magnon hybridization is confirmed in all samples of various thickness. We extracted the hybridization field and strength from the dispersion of all samples, as shown in Fig. 4(f); with the increase of the sample thickness, the coupling magnetic field increases monotonically, which is consistent with the trend of the saturation magnetic field (see Fig. S7 in the SM [42]), while the coupling strength increases first and then decreases with a small range of variation, indicating that the size of the magnetic vortex does not have a significant role in regulating the coupling strength. (More data for samples of other thicknesses at different  $\theta$  can be found in Sec. S9 in the SM [42].)

Apart from the apparent magnon hybridization of the low-frequency mode, we have found that there is also a weak hybridization at high frequencies  $\sim 8$  GHz from the experimental and simulation results, as shown in Figs. 4(c)–4(e). The appearance of the high-frequency mode was also presented in previous work [49], in which it was argued that, under longitudinal excitation, these modes are preferentially localized in the basic domains, where the local magnetization is perpendicular to the surface plane. Therefore, they label them as  $n$ -basic domain ( $n$ -BD) modes. On further reducing the applied field, the higher-order BD modes appear at specific values of the external field, and all of them are localized when they start to exist in the inner part of the stripes. We have investigated the magnon hybridization of the high-frequency mode using micromagnetic simulations with magnetic vortices (for more details, see Sec. S7 in the SM [42]). From

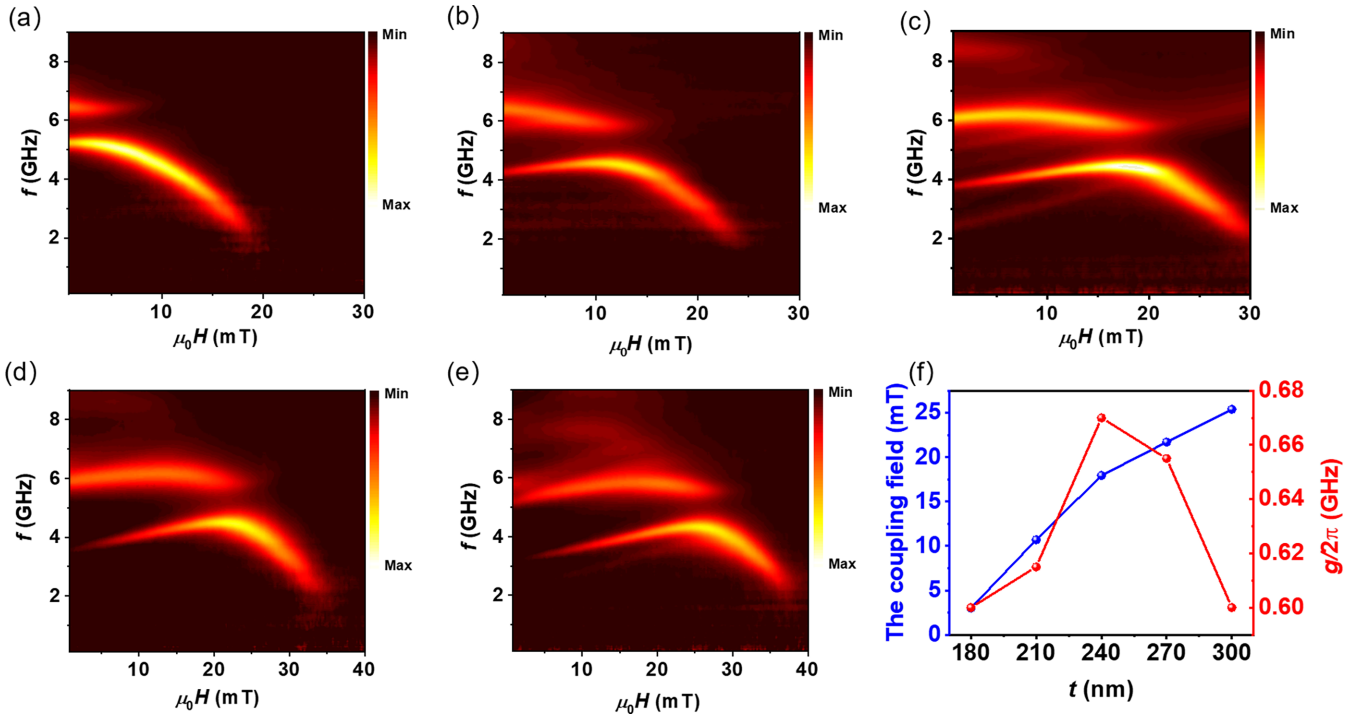


FIG. 4. Contour plots of measured permeability spectra for CoZr thin film with different thicknesses under the longitudinal excitation: (a) 180 nm, (b) 210 nm, (c) 240 nm, (d) 270 nm, and (e) 300 nm. (f) The coupling field and strength as a function of film thickness.

the simulation results, we speculate that the phenomenon under longitudinal excitation originates from the hybridization between the different modes of the overall precession of the magnetic moments, i.e., the higher-order magnon hybridization under longitudinal excitation originates from the

hybridization of the higher-order collective modes. The details could be studied in further work.

Additionally, to better understand the coupling phenomenon of the magnon hybridization in the magnetic vortex, we have also investigated the effect of different magnetic

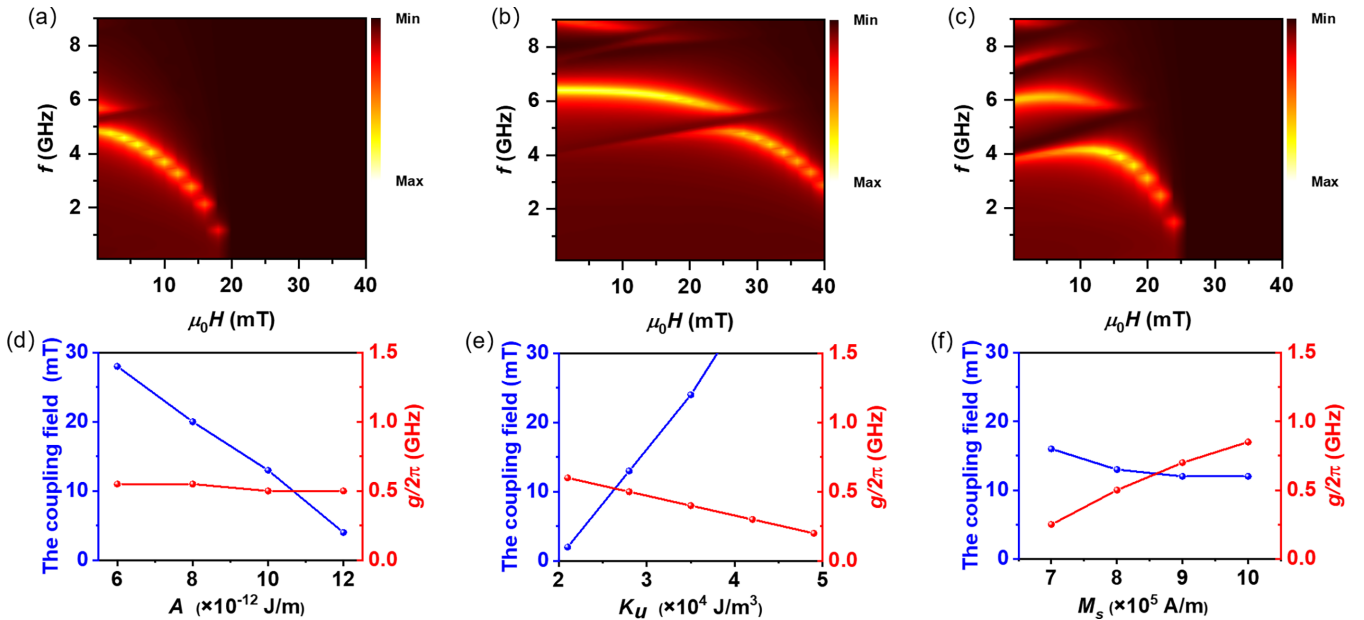


FIG. 5. Contour plots of simulated  $f$ - $H$  dispersion at different parameters compared with Fig. 2(b) under the longitudinal excitation. Fig. 2(b):  $A = 1.0 \times 10^{-11}$  J/m,  $K_u = 2.8 \times 10^4$  J/m<sup>3</sup>,  $M_s = 8 \times 10^5$  A/m, (a)  $A = 1.2 \times 10^{-11}$  J/m with  $M_s$  and  $K_u$  constant, (b)  $K_u = 4.2 \times 10^4$  J/m<sup>3</sup> with  $A$  and  $M_s$  constant, (c)  $M_s = 1 \times 10^6$  A/m with  $A$  and  $K_u$  constant. The coupling field and strength as a function of different parameters (d)  $A$ , (e)  $K_u$ , and (f)  $M_s$ .

parameters (exchange constant  $A$ , perpendicular magnetic anisotropy constant  $K_u$ , and saturation magnetization  $M_s$ ) on the coupling strength compared with Fig. 2(b) under the longitudinal excitation using micromagnetic simulations, as shown in Fig. 5. The parameters of Fig. 2(b) are  $A = 1.0 \times 10^{-11}$  J/m,  $K_u = 2.8 \times 10^4$  J/m<sup>3</sup>, and  $M_s = 8 \times 10^5$  A/m. Then we singly varied different  $A$ ,  $K_u$ , and  $M_s$ , respectively, where Figs. 5(a)–5(c) are  $A = 1.2 \times 10^{-11}$  J/m with  $M_s$  and  $K_u$  constant,  $K_u = 4.2 \times 10^4$  J/m<sup>3</sup> with  $A$  and  $M_s$  constant, and  $M_s = 1 \times 10^6$  A/m with  $A$  and  $K_u$  constant, respectively. (See Sec. S8 in the SM [42] for more details.) Extracting the data therein, we can obtain the relationship between the coupled magnetic field and strength with  $A$ ,  $K_u$ , and  $M_s$ , respectively, as shown in Figs. 5(d)–5(f). The coupled magnetic field decreases with the increase of  $A$ , while the coupling strength is almost constant, which is basically consistent with the variation in Fig. 4(f) because different domain widths have different  $A$ . With the increase of  $K_u$ , the coupled magnetic field gradually increases, while the coupling strength gradually decreases. With the increase of  $M_s$ , the coupled magnetic field slightly decreases, while the coupling strength monotonically increases. Therefore, to get a larger coupling strength in the experiment, we need to have a moderate  $K_u$  and a large  $M_s$ . This is certain guidance for the experiment.

## V. SUMMARY

In conclusion, the hybridization between different magnon modes of MVPs has been numerically and experimentally demonstrated. The simulation results demonstrated that the

observed hybridization is attributed to the coupling between the individual breathing mode and the collective mode of the MVP. Experimentally, we confirmed the magnon hybridization in CoZr thin films with striped domain by using longitudinal excited FMR measurement. It is further found that the hybridization is highly dependent on the size of magnetic vortex, which is experimentally confirmed by CoZr thin films with different thicknesses. Finally, it can be numerically obtained that the exchange constant does not affect the coupling strength, while the smaller the perpendicular magnetic anisotropy constant and the larger the saturation magnetization, the larger the coupling strength, which will have a certain guiding in enhancing the strength of the magnon hybridization of the MVP in the experiment. Our findings of the hybridization between different magnon modes of MVPs might open a way to study the interaction of magnons based on complex magnetic textures.

The data that support the findings of this paper are available from the corresponding author upon reasonable request.

## ACKNOWLEDGMENTS

This paper is supported by the National Natural Science Foundation of China (NSFC, Grants No. 12174165 and No. 12074189), the Natural Science Foundation of GanSu Province for Distinguished Young Scholars (Grant No. 20JR10RA649), and the Fundamental Research Funds for the Central Universities (Grant No. lzujbky-2022-kb06).

The authors have no conflicts to disclose.

- 
- [1] L.-Q. Dany, T. Yutaka, G. Arnaud, U. Koji, and N. Yasunobu, Hybrid quantum systems based on magnonics, *App. Phys. Express* **12**, 070101 (2019).
  - [2] Y. Li, W. Zhang, V. Tyberkevych, W.-K. Kwok, A. Hoffmann, and V. Novosad, Hybrid magnonics: Physics, circuits, and applications for coherent information processing, *J. Appl. Phys.* **128**, 130902 (2020).
  - [3] J. Xu, C. Zhong, X. Han, D. Jin, L. Jiang, and X. Zhang, Floquet cavity electromagnonics, *Phys. Rev. Lett.* **125**, 237201 (2020).
  - [4] Y. Xiao, X. H. Yan, L. H. Bai, H. Guo, C. M. Hu, and K. Xia, Magnon photon coupling for magnetization antiparallel to the magnetic field, *Phys. Rev. B* **103**, 104432 (2021).
  - [5] Y. Xiao, X. H. Yan, Y. Zhang, V. L. Grigoryan, C. M. Hu, H. Guo, and K. Xia, Magnon dark mode of an antiferromagnetic insulator in a microwave cavity, *Phys. Rev. B* **99**, 094407 (2019).
  - [6] P. Törmä and W. L. Barnes, Strong coupling between surface plasmon polaritons and emitters: A review, *Rep. Prog. Phys.* **78**, 013901 (2015).
  - [7] J. W. Rao, S. Kaur, X. L. Fan, D. S. Xue, B. M. Yao, Y. S. Gui, and C.-M. Hu, Characterization of the non-resonant radiation damping in coupled cavity photon magnon system, *Appl. Phys. Lett.* **110**, 262404 (2017).
  - [8] D. S. Dovzhenko, S. V. Ryabchuk, Yu. P. Rakovich, and I. R. Nabiev, Light-matter interaction in the strong coupling regime: Configurations, conditions, and applications, *Nanoscale* **10**, 3589 (2018).
  - [9] P. Sivarajah, A. Steinbacher, B. Dastrup, J. Lu, M. Xiang, W. Ren, S. Kamba, S. Cao, and K. A. Nelson, THz-frequency magnon-phonon-polaritons in the collective strong-coupling regime, *J. Appl. Phys.* **125**, 213103 (2019).
  - [10] Z. Zhang, M. O. Scully, and G. S. Agarwal, Quantum entanglement between two magnon modes via Kerr nonlinearity driven far from equilibrium, *Phys. Rev. Res.* **1**, 023021 (2019).
  - [11] K. Ma, C. Li, Z. Hao, C. K. Ong, and G. Chai, Strong magnon-magnon coupling between ferromagnetic resonances in Co<sub>90</sub>Zr<sub>10</sub>/Ta/Fe<sub>20</sub>Ni<sub>80</sub> multilayers, *Phys. Rev. B* **108**, 094422 (2023).
  - [12] S. Klingler, V. Amin, S. Geprägs, K. Ganzhorn, H. Maier-Flaig, M. Althammer, H. Huebl, R. Gross, R. D. McMichael, M. D. Stiles *et al.*, Spin-torque excitation of perpendicular standing spin waves in coupled YIG/Co heterostructures, *Phys. Rev. Lett.* **120**, 127201 (2018).
  - [13] J. Inman, Y. Xiong, R. Bidthanapally, S. Louis, V. Tyberkevych, H. Qu, J. Sklenar, V. Novosad, Y. Li, X. Zhang *et al.*, Hybrid magnonics for short-wavelength spin waves facilitated by a magnetic heterostructure, *Phys. Rev. Appl.* **17**, 044034 (2022).
  - [14] Y. Xiong, J. Inman, Z. Li, K. Xie, R. Bidthanapally, J. Sklenar, P. Li, S. Louis, V. Tyberkevych, H. Qu *et al.*, Tunable magnetically induced transparency spectra in magnon-magnon coupled

- $\text{Y}_3\text{Fe}_5\text{O}_{12}$ /permalloy bilayers, *Phys. Rev. Appl.* **17**, 044010 (2022).
- [15] Y. Shiota, T. Taniguchi, M. Ishibashi, T. Moriyama, and T. Ono, Tunable magnon-magnon coupling mediated by dynamic dipolar interaction in synthetic antiferromagnets, *Phys. Rev. Lett.* **125**, 017203 (2020).
- [16] M. Li, J. Lu, and W. He, Symmetry breaking induced magnon-magnon coupling in synthetic antiferromagnets, *Phys. Rev. B* **103**, 064429 (2021).
- [17] A. Sud, C. W. Zollitsch, A. Kamimaki, T. Dion, S. Khan, S. Iihama, S. Mizukami, and H. Kurebayashi, Tunable magnon-magnon coupling in synthetic antiferromagnets, *Phys. Rev. B* **102**, 100403(R) (2020).
- [18] D. MacNeill, J. T. Hou, D. R. Klein, P. Zhang, P. Jarillo-Herrero, and L. Liu, Gigahertz frequency antiferromagnetic resonance and strong magnon-magnon coupling in the layered crystal  $\text{CrCl}_3$ , *Phys. Rev. Lett.* **123**, 047204 (2019).
- [19] L. Liensberger, A. Kamra, H. Maier-Flaig, S. Geprägs, A. Erb, S. T. B. Goennenwein, R. Gross, W. Belzig, H. Huebl, and M. Weiler, Exchange-enhanced ultrastrong magnon-magnon coupling in a compensated ferrimagnet, *Phys. Rev. Lett.* **123**, 117204 (2019).
- [20] N. Nishimura, T. Hirai, A. Koganei, T. Ikeda, K. Okano, Y. Sekiguchi, and Y. Osada, Magnetic tunnel junction device with perpendicular magnetization films for high-density magnetic random access memory, *J. Appl. Phys.* **91**, 5246 (2002).
- [21] C. A. Ross, Patterned magnetic recording media, *Annu. Rev. Mater. Res.* **31**, 203 (2001).
- [22] R. P. Cowburn and M. E. Welland, Room temperature magnetic quantum cellular automata, *Science* **287**, 1466 (2000).
- [23] A. Khitun, M. Bao, and K. L. Wang, Magnonic logic circuits, *J. Phys. D: Appl. Phys.* **43**, 264005 (2010).
- [24] Y. Shen, X. Wang, Z. Xie, C. Min, X. Fu, Q. Liu, M. Gong, and X. Yuan, Optical vortices 30 years on: OAM manipulation from topological charge to multiple singularities, *Light: Sci. & Appl.* **8**, 90 (2019).
- [25] M. Brambilla, F. Battipede, L. A. Lugiato, V. Penna, F. Prati, C. Tamm, and C. O. Weiss, Transverse laser patterns. I. Phase singularity crystals, *Phys. Rev. A* **43**, 5090 (1991).
- [26] I. S. Aranson and L. Kramer, The world of the complex Ginzburg-Landau equation, *Rev. Mod. Phys.* **74**, 99 (2002).
- [27] Q. Li, V. A. Stoica, M. Paściak, Y. Zhu, Y. Yuan, T. Yang, M. R. McCarter, S. Das, A. K. Yadav, S. Park *et al.*, Subterahertz collective dynamics of polar vortices, *Nature (London)* **592**, 376 (2021).
- [28] I. Luk'yanchuk and V. M. Vinokur, Dynamics of ferroelectric vortices revealed, *Nature (London)* **592**, 359 (2021).
- [29] M. Y. Im, P. Fischer, K. Yamada, T. Sato, S. Kasai, Y. Nakatani, and T. Ono, Symmetry breaking in the formation of magnetic vortex states in a permalloy nanodisk, *Nat. Commun.* **3**, 983 (2012).
- [30] A. Bogdanov and A. Hubert, Thermodynamically stable magnetic vortex states in magnetic crystals, *J. Magn. Magn. Mater.* **138**, 255 (1994).
- [31] R. Antos, Y. C. Otani, and J. Shibata, Magnetic vortex dynamics, *J. Phys. Soc. of Jpn.* **77**, 031004 (2008).
- [32] M. M. Salomaa and G. E. Volovik, Vortices with ferromagnetic superfluid core in  $^3\text{He-B}$ , *Phys. Rev. Lett.* **51**, 2040 (1983).
- [33] J. Shibata and Y. Otani, Magnetic vortex dynamics in a two-dimensional square lattice of ferromagnetic nanodisks, *Phys. Rev. B* **70**, 012404 (2004).
- [34] V. Novosad, M. Grimsditch, K. Yu. Guslienko, P. Vavassori, Y. Otani, and S. D. Bader, Spin excitations of magnetic vortices in ferromagnetic nanodots, *Phys. Rev. B* **66**, 052407 (2002).
- [35] B. A. Ivanov and C. E. Zaspel, High frequency modes in vortex-state nanomagnets, *Phys. Rev. Lett.* **94**, 027205 (2005).
- [36] Y. Onose, Y. Okamura, S. Seki, S. Ishiwata, and Y. Tokura, Observation of magnetic excitations of skyrmion crystal in a helimagnetic insulator  $\text{Cu}_2\text{OSeO}_3$ , *Phys. Rev. Lett.* **109**, 037603 (2012).
- [37] M. Mochizuki, Spin-wave modes and their intense excitation effects in skyrmion crystals, *Phys. Rev. Lett.* **108**, 017601 (2012).
- [38] M. Mruczkiewicz, M. Krawczyk, and K. Y. Guslienko, Spin excitation spectrum in a magnetic nanodot with continuous transitions between the vortex, Bloch-type skyrmion, and Néel-type skyrmion states, *Phys. Rev. B* **95**, 094414 (2017).
- [39] Y. Ma, C. Song, C. Jin, J. Wang, H. Xia, Y. Wei, J. Wang, and Q. Liu, Microwave-driven dynamic switching of the radial vortex in a nanodot by micromagnetic simulation, *J. Phys. D: Appl. Phys.* **52**, 195001 (2019).
- [40] G. Siracusano, R. Tomasello, A. Giordano, V. Puliafito, B. Azzerboni, O. Ozatay, M. Carpentieri, and G. Finocchio, Magnetic radial vortex stabilization and efficient manipulation driven by the Dzyaloshinskii-Moriyai interaction and spin-transfer torque, *Phys. Rev. Lett.* **117**, 087204 (2016).
- [41] B. A. Ivanov and C. E. Zaspel, Magnon modes for thin circular vortex-state magnetic dots, *App. Phys. Lett.* **81**, 1261 (2002).
- [42] See Supplemental Material at <http://link.aps.org/supplemental/10.1103/PhysRevB.109.214437> for more details about the magnetization distributions and dispersion relations obtained by micromagnetic simulations of single magnetic vortex with different chirality and the MVP at different magnetic vortex spacing; experimental contour plots of  $f-H$  dispersion for different angles of applied dc and microwave magnetic fields with different CoZr thin films thickness; the magnetization hysteresis loops, magnetic domain images, and half width of the magnetic domains of CoZr thin films with different thicknesses; and which includes Refs. [36,41,48,54].
- [43] N. Vukadinovic, O. Vacus, M. Labrune, O. Acher, and D. Pain, Magnetic excitations in a weak-stripe-domain structure: A 2D dynamic micromagnetic approach, *Phys. Rev. Lett.* **85**, 2817 (2000).
- [44] J. Yu, X. Chen, F. Wang, R. Adam, D. E. Bürgler, L. Pan, J. Zhang, Y. Cui, Q. Li, M. Liu *et al.*, Magnetization enhanced the multiple magnetic domain-dominated resonance modes in stripe domain films, *New J. Phys.* **25**, 013008 (2023).
- [45] N. Vukadinovic, H. L. Gall, J. B. Youssef, V. Gehanno, A. Marty, Y. Samson, and B. Gilles, Magnetization dynamics and relaxation in epitaxial FePd thin films with a stripe domain structure, *Eur. Phys. J. B* **13**, 445 (2000).
- [46] U. Ebels, L. Buda, and K. Ounadjela, and P. E. Wigen, Ferromagnetic resonance excitation of two-dimensional wall structures in magnetic stripe domains, *Phys. Rev. B* **63**, 174437 (2001).
- [47] C. Banerjee, P. Gruszecki, J. W. Klos, O. Hellwig, M. Krawczyk, and A. Barman, Magnonic band structure in a Co/Pd stripe domain system investigated by Brillouin light

- scattering and micromagnetic simulations, *Phys. Rev. B* **96**, 024421 (2017).
- [48] N. Vukadinovic, M. Labrune, J. B. Youssef, A. Marty, J. C. Toussaint, and H. L. Gall, Ferromagnetic resonance spectra in a weak stripe domain structure, *Phys. Rev. B* **65**, 054403 (2001).
- [49] I. S. Camara, S. Tacchi, L.-C. Garnier, M. Eddrief, F. Fortuna, G. Carlotti, and M. Marangolo, Magnetization dynamics of weak stripe domains in Fe-N thin films: A multi-technique complementary approach, *J. Phys.: Condens. Matter* **29**, 465803 (2017).
- [50] A. Vansteenkiste, J. Leliaert, M. Dvornik, M. Helsen, F. Garcia-Sanchez, and B. Van Waeyenberge, The design and verification of MUMAX3, *AIP Adv.* **4**, 107133 (2014).
- [51] Y. Ding, T. J. Klemmer, and T. M. Crawford, A coplanar waveguide permeameter for studying high-frequency properties of soft magnetic materials, *J. Appl. Phys.* **96**, 2969 (2004).
- [52] Y. Liu, L. F. Chen, C. Y. Tan, H. J. Liu, and C. K. Ong, Broadband complex permeability characterization of magnetic thin films using shorted microstrip transmission-line perturbation, *Rev. Sci. Instrum.* **76**, 063911 (2005).
- [53] Z. Zhang, L. Zhou, P. E. Wigen, and K. Ounadjelaz, Using ferromagnetic resonance as a sensitive method to study temperature dependence of interlayer exchange coupling, *Phys. Rev. Lett.* **73**, 336 (1994).
- [54] H. Ma, C. Li, W. Wang, and G. Chai, Thickness-dependent resonance frequency of non-uniform procession mode in CoZr stripe domain magnetic films, *J. Phys. D: Appl. Phys.* **51**, 285004 (2018).